REFERENCES

[1] S. E. Miller, "Integrated optics: An introduction," *Bell Syst. Tech. J.*, vol. 48, p. 2059, Sept. 1969.
[2] D. Marcuse, *Light Transmission Optics*. New York: Van Nostrand Reinhold, 1972.
[3] H. Kogelnik, "An introduction to integrated optics," *IEEE Trans. Microwave Theory Tech.*, vol. MTT-23, p. 2, Jan. 1975.
[4] P. K. Tien, "Light waves in thin films and integrated optics," *Appl. Opt.*, vol. 10, p. 2395, Nov. 1971.
[5] N. G. Alexopoulos and S. R. Kerner, "A coupled-power theorem and orthogonality relations for optical disk waveguides," *J. Opt. Soc. Amer.*, vol. 67, no. 12, Dec. 1977.
[6] S. R. Kerner, "Characteristics of radial dielectric waveguides," M.S. thesis, Univ. California, Los Angeles, 1977.
[7] M. Abramowitz and I. Stegun, *Handbook of Mathematical Functions*, ninth printing, Applied Mathematics Series-55, U.S. Government Printing Office, Washington, DC, 1970.

Scattering from an Arbitrarily Located Off-Axis Inhomogeneity in a Step-Index Optical Fiber

AHMAD SAFAAI-JAZI AND GAR LAM YIP, SENIOR MEMBER, IEEE

Abstract—**An exact analysis using the Green's function formulation of an arbitrarily oriented off-axis dipole radiating into a dielectric rod waveguide is carried out. The method of analysis involves expressing the fields and the current source in a Fourier integral in the z-direction and a Fourier series in the ϕ-direction in a cylindrical coordinate system (ρ, ϕ, z). The practical significance of this analysis, in particular with regard to its applications to the problem of scattering from an arbitrarily located inhomogeneity in a step-index optical fiber, is presented.**

I. INTRODUCTION

DIELECTRIC optical waveguides are receiving ever increasing attention recently. Although much effort has been devoted to further developing the optical fiber theory in recent years, there still remain certain problems which deserve more detailed studies. One problem of considerable importance is the excitation of guided modes and radiation by infinitesimal dipole sources in cylindrically stratified dielectric waveguides. A rigorous mathematical treatment of the problem necessitates solving an inhomogeneous wave equation.

A comprehensive treatment of excitation problems involving point and line sources in the presence of dielectric slab waveguides can be found in [1] and [2]. A similar problem in the case of cylindrical dielectric waveguides involves a much greater degree of mathematical complexity, and, except for certain special cases, a general solution to the excitation problem has not been available so far. Duncan [3] and Brown and Stachera [4] have studied the excitation of the TM_{01} mode on a dielectric rod by a magnetic current ring, while Yip [5] investigated the excitation of the HE_{11} mode by a transversely oriented infinitesimal dipole on the axis of a rod.

The treatment of an arbitrarily oriented off-axis dipole is somewhat complicated, especially when the radiation fields are to be determined. Fortunately, the surface-wave fields can be evaluated by employing the Lorentz reciprocity theorem involving the use of the orthogonality relations in the modal fields without solving the entire excitation problem. The analysis was first carried out by Goubau [6] and is also outlined in [7]. This method has been used to study the mode conversion due to scattering by localized inhomogeneities in optical fibers [8] and [9].

This method, while successful in handling the guided modes, does not yield any information about the radiation fields which are also excited by a scatterer. For waveguides with small dielectric difference between the core and the cladding, the radiation loss due to localized impurities can be approximated by the power radiated from an equivalent dipole into an infinite homogeneous medium with a permittivity equal to that of the medium

Manuscript received January 23, 1978; revised September 19, 1978. This paper was presented at the International Microwave Symposium, June 27–29, 1978, Ottawa, Ont., Canada, Session on "Fiber and Integrated Optics". This research was supported by the National Research Council of Canada.

The authors are with the Department of Electrical Engineering, McGill University, Montreal, P.Q., Canada H3A 2A7.

0018-9480/80/0100-0024$00.75 ©1980 IEEE

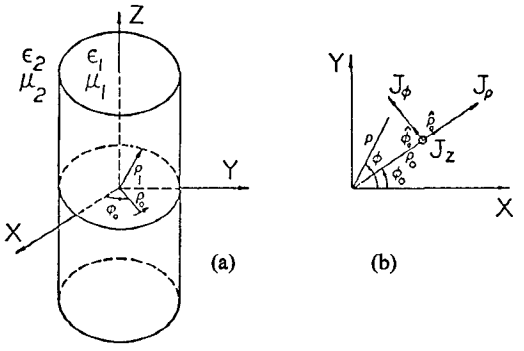

Fig. 1. Geometry of the problem. (a) The dielectric rod and the point dipole. (b) Current components in the dipole.

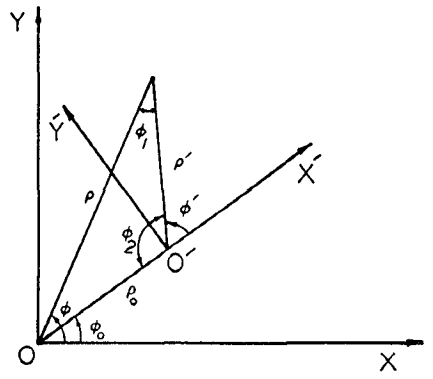

Fig. 2. Transformation of coordinates in the $z=0$ plane.

surrounding the dipole [9]. But this approximation cannot take into consideration the boundary between the core and the cladding. Moreover, the calculated power becomes less and less accurate as the dielectric difference between the core and the cladding increases.

The aim of this paper is to present a rigorous Green's function analysis of an off-axis and arbitrarily oriented dipole in a two-layer cylindrical dielectric waveguide. The treatment allows both the radiation fields and guided modes to be examined. The method of analysis involves a Fourier transform technique in conjunction with a coordinate transformation and the application of the Graf's formula [10]. Solutions for the far zone radiation fields and surface-wave fields for all modes and the corresponding powers are obtained. These solutions are then used to study, in detail, radiation and mode conversion losses due to scattering from a discrete and randomly situated scatterer in a dielectric-rod optical waveguide in which the dominant HE_{11} mode propagates.

II. Formulation of the Problem

Consider a cylindrical dielectric waveguide composed of a core with a radius ρ_1 and an infinite cladding as illustrated in Fig. 1(a). The core and cladding are characterized by permittivities $\epsilon_1=\epsilon_0\epsilon_{r1}$ and $\epsilon_2=\epsilon_0\epsilon_{r2}$ and permeabilities $\mu_1=\mu_0\mu_{r1}$ and $\mu_2=\mu_0\mu_{r2}$, respectively. A cylindrical coordinate system (ρ,ϕ,z) with the z-axis coinciding with the axis of the core is chosen. A point electric dipole with an arbitrary orientation is placed at (ρ_0,ϕ_0,z_0). The time variation is assumed to be of the form $\exp(-j\omega t)$ which will be omitted throughout the analysis. Without loss of generality, z_0 is set to zero. The current density in the dipole is expressed as a three-dimensional delta function given by

$$\vec{J}_1=\left(J_\rho\hat{\rho}_0+J_\phi\hat{\phi}_0+J_z\hat{z}_0\right)\delta(\vec{\rho}-\vec{\rho}_0) \tag{1a}$$

where

$$\delta(\vec{\rho}-\vec{\rho}_0)=\begin{cases}\delta(\rho-\rho_0)\delta(\phi-\phi_0)\delta(z)/\rho, & \rho_0>0\\ \delta(\rho)\delta(z)/2\pi\rho, & \rho_0=0\end{cases} \tag{1b}$$

and $\hat{\rho}_0$, $\hat{\phi}_0$, and $\hat{z}_0$ are unit vectors at ρ_0, ϕ_0, and z_0, along the radial, azimuthal, and axial directions, respectively, as indicated in Fig. 1 (b). Decomposing $\vec{J}_1$ along some arbitrary directions $\hat{\rho}$ and $\hat{\phi}$ yields

$$\vec{J}_1=\left\{\left[J_\rho\cos(\phi-\phi_0)+J_\phi\sin(\phi-\phi_0)\right]\hat{\rho}+\left[J_\phi\cos(\phi-\phi_0)-J_\rho\sin(\phi-\phi_0)\right]\hat{\phi}+J_z\hat{z}\right\}\delta(\vec{\rho}-\vec{\rho}_0). \tag{2}$$

Let us assume, for the time being, that $\rho_0<\rho_1$; i.e., the dipole is in the core region. The wave equations can be written as

$$\left(\nabla^2+k_0^2\mu_{r1}\epsilon_{r1}\right)\begin{bmatrix}\vec{H}\\ \vec{E}\end{bmatrix}=\begin{cases}-\nabla\times\vec{J}\\ -j\left(k_0\mu_{r1}\vec{J}+\nabla\nabla\cdot\vec{J}/k_0\epsilon_{r1}\right),\end{cases}\qquad 0\leqslant\rho\leqslant\rho_1 \tag{3a}$$

$$\left(\nabla^2+k_0^2\mu_{r2}\epsilon_{r2}\right)\begin{bmatrix}\vec{H}\\ \vec{E}\end{bmatrix}=0,\qquad \rho\geqslant\rho_1 \tag{3b}$$

where $\vec{E}=(\epsilon_0)^{1/2}\vec{E}_1$, $\vec{H}=(\mu_0)^{1/2}\vec{H}_1$, and $\vec{J}=(\mu_0)^{1/2}\vec{J}_1$ are the normalized fields and current density. The case $\rho_0>\rho_1$, that is when the dipole is in the cladding region, will be discussed later. The technique used for solving the inhomogeneous wave (3a) involves the following steps: 1) a coordinate transformation in the $z=0$ plane such that the new origin is at $(\rho_0,\phi_0,0)$ and the new x-axis; i.e., x'-axis makes an angle ϕ_0 with the old x-axis as shown in Fig. 2. 2) transformation of the fields and the current density by means of a Fourier transform integral from the z domain into the $\bar{\beta}$ domain, $\bar{\beta}=\beta/k_0$ being the normalized axial propagation constant.

Following step 1), the new transverse coordinates in terms of the old ones are given by

$$\rho'=\left[\rho^2+\rho_0^2-2\rho\rho_0\cos(\phi-\phi_0)\right]^{1/2}$$
$$\phi'=\phi-\phi_0+\phi_1=\pi-\phi_2. \tag{4}$$

The current density $\vec{J}$ in the new coordinate system becomes

$$\vec{J}=(\mu_0)^{1/2}\left[\left(J_\rho\cos\phi'+J_\phi\sin\phi'\right)\hat{\rho}'+\left(J_\phi\cos\phi'-J_\rho\sin\phi'\right)\hat{\phi}'+J_z\hat{z}\right]\delta(\rho')\delta(z)/2\pi\rho'. \tag{5}$$

It should be noted that (3a) and (3b), as they stand, are valid in the new coordinate system too. By means of a

Fourier transform integral the fields and the current density components can be expressed in the following form:

$$F(\rho',\phi',\bar{\beta}) = \int_{-\infty}^{\infty} f(\rho',\phi',z)\exp(-jk_0\bar{\beta}z)\,dz. \quad (6)$$

Using (5) and (6) in (3a), the following wave equations for the transformed axial components of the fields are obtained

$$(\nabla_t^2 + k_1^2)\begin{bmatrix} H_{z1}(\rho',\phi',\bar{\beta}) \\ E_{z1}(\rho',\phi',\bar{\beta}) \end{bmatrix} = \begin{cases} -\dfrac{j(\mu_0)^{1/2}}{4\pi}, \dfrac{d}{d\rho'}\left[\dfrac{\delta(\rho')}{\rho'}\right] \displaystyle\sum_{m=1,-1} m(J_\rho - jmJ_\phi)\exp(jm\phi') \\ (\mu_0)^{1/2}\left\{-\dfrac{jk_1^2 J_z}{2\pi k_0\epsilon_{r1}}\cdot\dfrac{\delta(\rho')}{\rho'} + \dfrac{\bar{\beta}}{4\pi\epsilon_{r1}} \cdot\dfrac{d}{d\rho'}\left[\dfrac{\delta(\rho')}{\rho'}\right]\displaystyle\sum_{m=1,-1}(J_\rho - jmJ_\phi)\exp(jm\phi')\right\} \end{cases} \quad (7)$$

where $k_1^2 = k_0^2(\mu_{r1}\epsilon_{r1} - \bar{\beta}^2)$. The corresponding equations for $H_{z2}(\rho',\phi',\bar{\beta})$ and $k_{z2}(\rho',\phi',\bar{\beta})$, the axial components in the cladding region, are obtained from (7) by setting the right hand side expressions to zero and replacing the subscript 1 by 2 in all relevant terms. The particular solutions to the inhomogeneous equations in (7) can be written

$$H_{z1}^p(\rho',\phi',\bar{\beta}) = T_0 \sum_{m=1,-1}\left(\tfrac{1}{2}\right) \cdot(J_\rho - jmJ_\phi)\,Y_m(k_1\rho')\exp(jm\phi') \quad (8a)$$

$$E_{z1}^p(\rho',\phi',\bar{\beta}) = T_0\Big[-(J_z k_1/k_0\epsilon_{r1})\,Y_0(k_1\rho') + \sum_{m=1,-1}\left(jm\bar{\beta}/2\epsilon_{r1}\right) \cdot(J_\rho - jmJ_\phi)\cdot Y_m(k_1\rho')\exp(jm\phi')\Big] \quad (8b)$$

where $T_0 = jk_1(\mu_0)^{1/2}/4$ and J_m and Y_m are the Bessel functions of the first and second kinds, respectively. It is now appropriate to write these solutions in terms of the old coordinates ρ and ϕ. In doing so, we make use of the Graf's formula [10] expressed as

$$\exp(j\nu\phi_1)Z_\nu(k_1\rho') = \sum_{n=-\infty}^{\infty} z_{n+\nu}(k_1\rho)J_n(k_1\rho_0)\exp(jn\Omega) \quad (9)$$

where $Z_n = J_n$, Y_n, $H_n^{(1)}$, or $H_n^{(2)}$ and ρ, ρ_0, and ρ' $[=(\rho^2+\rho_0^2-2\rho\rho_0\cos\Omega)^{1/2}$ with $|\rho| > |\rho_0|]$ form a triangle with $\Omega = \phi - \phi_0$ as seen in Fig. 2. Hence, with the help of (9) and taking into account the solutions to the homogeneous equations in (7), the following results for the complete solutions are obtained.

$$\begin{cases} E_{z1}(\rho,\phi,\bar{\beta}) = \displaystyle\sum_{n=-\infty}^{\infty}\left[(R_n + a_{n1})J_n(k_1\rho)\right]F_n \\ H_{z1}(\rho,\phi,\bar{\beta}) = \displaystyle\sum_{n=-\infty}^{\infty}\left[(S_n + b_{n1})J_n(k_1\rho)\right]F_n \end{cases}, \quad 0 \leqslant \rho \leqslant \rho_0, \quad (10a)$$

$$\begin{cases} E_{z1}(\rho,\phi,\bar{\beta}) = \displaystyle\sum_{n=-\infty}^{\infty}\left[R_n' Y_n(k_1\rho) + a_{n1}J_n(k_1\rho)\right]F_n \\ H_{z1}(\rho,\phi,\bar{\beta}) = \displaystyle\sum_{n=-\infty}^{\infty}\left[S_n' Y_n(k_1\rho) + b_{n1}J_n(k_1\rho)\right]F_n \end{cases}, \quad \rho_0 \leqslant \rho \leqslant \rho_1 \quad (10b)$$

$$\begin{cases} E_{z2}(\rho,\phi,\bar{\beta}) = \displaystyle\sum_{n=-\infty}^{\infty} a_{n2}H_n^{(1)}(k_2\rho)F_n \\ H_{z2}(\rho,\phi,\bar{\beta}) = \displaystyle\sum_{n=-\infty}^{\infty} b_{n2}H_n^{(1)}(k_2\rho)F_n \end{cases}, \quad \rho \geqslant \rho_1 \quad (10c)$$

where $k_2 = k_0(\mu_{r2}\epsilon_{r2} - \bar{\beta}^2)^{1/2}$ and $F_n = \exp[jn(\phi - \phi_0)]$. In (10), the coefficients R_n, S_n, R_n', S_n' are associated with solutions to the inhomogeneous equations, whereas the unknown coefficients a_{n1}, b_{n1}, a_{n2}, and b_{n2} can be determined by imposing the boundary conditions at the core–cladding interface. For brevity, detailed expressions for these coefficients are not given here, but can be found in [11].

III. Evaluation of Actual Fields

The actual field components are obtained by Fourier transforming the fields in the $\bar{\beta}$ domain according to

$$f(\rho,\phi,z) = \frac{k_0}{2\pi}\int_{-\infty}^{\infty} F(\rho,\phi,\bar{\beta})\exp(jk_0\bar{\beta}z)\,d\bar{\beta} \quad (11)$$

where f represents a component of the electric or magnetic field in the z domain and F is the corresponding component in the $\bar{\beta}$ domain. The evaluation of the integral in (11) is performed by means of a contour integration. In doing so, the analyticity of the integrands involved must be first investigated. In other words, the singularities of the integrands, namely poles and branch points should be determined. An examination of field coefficients in (10) reveals that the poles are the real roots of the characteristic equation $\Delta(\bar{\beta}) = 0$. To identify the branch points, let us first consider the variable k_2 which appears in the argument of the Hankel function. k_2 is clearly multivalued in the neighborhood of $\bar{\beta} = \pm\bar{\beta}_r$, where $\bar{\beta}_r = (\mu_{r2}\epsilon_{r2})^{1/2}$. Moreover, the series expansion of the Hankel function has a logarithmic term, and is thus singular at $k_2 = 0$. Consequently, $\bar{\beta} = \pm\bar{\beta}_r$ are branch points from which the cuts are taken. The possibility of branch points at $\bar{\beta} = \pm(\mu_{r1}\epsilon_{r1})^{1/2}$ may be questioned because of the presence of the multivalued variable k_1 in the arguments of the Bessel function J_n and Y_n and the logarithmic singularity inherent in Y_n. It can be proved [11] that if k_1 is replaced by $k_1\cdot\exp(j\pi)$, the integrands remain unchanged. Further,

their series expansions are free from any logarithmic singularity. Hence, $\bar{\beta}=\pm(\mu_{r1}\epsilon_{r1})^{1/2}$ are not branch points. Then, the contour of integration, as shown in Fig. 3, is so constructed that the singularities are avoided. By the residue theorem

$$\int_{-\infty}^{\infty} = -\int_{C_1} - \int_{C_2} + 2\pi j \sum \text{ Residues.} \tag{12}$$

In (12), the integral along C_1 vanishes as the radius of C_1 approaches infinity. The integral along C_2, the branch cut, contributes to the radiation fields, while the sum of the residues which corresponds to the contribution of the poles accounts for the surface-wave fields.

A. Radiation Fields

The radiation fields are obtained by evaluating the branch cut integral in (12). The exact evaluation of this integral is a formidable task. In the far zone where ρ and z are sufficiently large, however, an asymptotic evaluation of the integral is possible by means of a saddle point method of integration [1] and [3]. To facilitate the asymptotic evaluation of the branch cut integral, it is desirable to introduce the transformation $\bar{\beta}=\bar{\beta}_r\cos\tau$. It is further convenient to utilize the spherical coordinates (r,ϕ,θ) where θ is measured from the z-axis so that $\rho=r\sin\theta$ and $z=r\cos\theta$. Applying the above mentioned transformation, using the large argument approximation of the Hankel function in (10c) and (12), and deforming the contour C_τ in the τ plane which is transformed from C_2 in the $\bar{\beta}$ plane, into a steepest descent path passing through the saddle point at $\tau=\theta$, one obtains,

$$\begin{bmatrix} E_\phi(r,\phi,\theta) \\ H_\phi(r,\phi,\theta) \end{bmatrix} = \sum_{n=-\infty}^{\infty} j \begin{bmatrix} (\mu_{r2}/\epsilon_{r2})^{1/2} & b_{n2}(\theta) \\ -(\epsilon_{r2}/\mu_{r2})^{1/2} & a_{n2}(\theta) \end{bmatrix} \frac{1}{\sin\theta} \cdot \exp\left[jn\left(\phi-\phi_0-\pi/2\right)\right] \cdot \frac{\exp\left(jk_0\beta_r\right)}{\pi r} \tag{13}$$

$$E_\theta(r,\phi,\theta)=(\mu_{r2}/\epsilon_{r2})^{1/2}\cdot H_\phi(r,\phi,\theta) \tag{14a}$$

$$H_\theta(r,\phi,\theta)=-(\epsilon_{r2}/\mu_{r2})^{1/2}\cdot E_\phi(r,\phi,\theta). \tag{14b}$$

In (13), $a_{n2}(\theta)$ and $b_{n2}(\theta)$ are obtained from a_{n2} and b_{n2} in (10) replacing $\bar{\beta}$ by $\bar{\beta}_r\cos\theta$.

The radiation power is determined by integrating the real part of one-half of the radial component of the complex Poynting vector over a sphere of an arbitrarily large radius.

$$P_r=\frac{1}{2(\mu_0\epsilon_0)^{1/2}}\int_0^{2\pi}\int_0^{\pi} P(r,\phi,\theta)r^2\sin\theta\,d\phi\,d\theta \tag{15a}$$

where

$$P(r,\phi,\theta)=\text{Re}\left[E_\theta(r,\phi,\theta)H_\phi^*(r,\phi,\theta) - E_\phi(r,\phi,\theta)H_\theta^*(r,\phi,\theta)\right]. \tag{15b}$$

Substituting for E_θ, H_θ, E_ϕ, and H_ϕ from (13) and (14), the radiated power is obtained, after some simplifications, as

$$P_r=\frac{4}{\pi\sqrt{\mu_0\epsilon_0}}\sum_{n=0}^{\infty}\int_0^{\bar{\beta}_r}\kappa_n|\Gamma_n|^2\left[\epsilon_{r2}\left(|a_n^z|^2+|a_n^\rho|^2+|a_n^\phi|^2\right) + \mu_{r2}\left(|b_n^z|^2+|b_n^\rho|^2+b_n^\phi|^2\right)\right]\frac{d\bar{\beta}}{\bar{\beta}_r^2-\bar{\beta}^2} \tag{16a}$$

where

$$a_n=T_0\left(a_n^z+a_n^\rho+a_n^\phi\right)$$
$$b_n=T_0\left(b_n^z+b_n^\rho+b_n^\phi\right) \tag{16b}$$

a_n and b_n are factors contained in $a_{n1}, b_{n1}, a_{n2}, b_{n2}$, $K_n=1/2$ for $n=0$, $K_n=1$ for $n>0$, $\Gamma_n=\Delta_0 T_0/H_n^{(1)}(w)$, $\Delta_0=-2/[\pi x^2 J_n(x)\Delta(\bar{\beta})]$, $x=k_1\rho_1$, and $w=k_2\rho_1$. The detailed expressions for the terms in (16b) can again be found in [11]. The infinite series in (16a) is absolutely convergent, since the ratio of the $(n+1)$th term to the nth one goes to zero as n approaches infinity.

The radiation pattern may be obtained from $|P(r,\phi,\theta)|$, given by (15b). In general, when all current components J_z, J_ρ, and J_ϕ are present and $\rho_0>0$, there is no symmetry in the radiation pattern. For special cases such as an on-axis dipole ($\rho_0=0$), to be discussed later, a great deal of simplification occurs in both radiated power and radiation pattern.

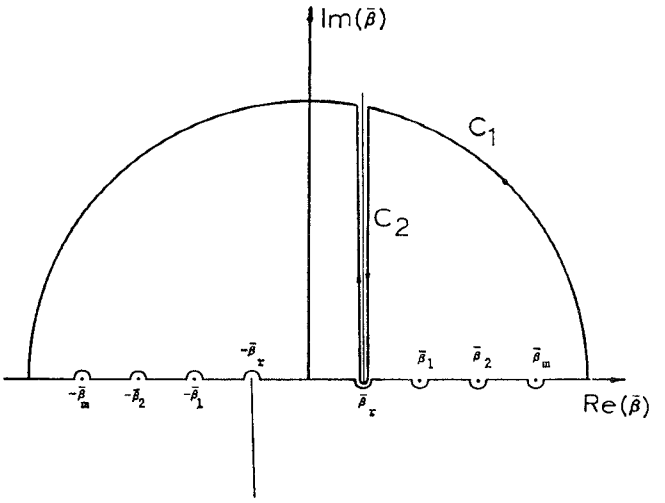

Fig. 3. Contour of integration in the complex $\bar{\beta}$ plane.

B. Surface-Wave Fields

For propagation in the positive z-direction, the surface-wave fields for a particular mode having an azimuthal number n are obtained by evaluating the residues at the pole corresponding to the mode concerned. Hence, from (10) and with the help of (11) and (12), the following results are obtained. For $n\geq 1$

$$\begin{cases} E_{z1,n}(\rho,\phi,z)=\bar{A}_n J_n(k_1\rho)\bar{F}_n \\ H_{z1,n}(\rho,\phi,z)=j\bar{A}_n\Omega_1 J_n(k\rho)\bar{F}_n \end{cases}, \quad 0\leq\rho\leq\rho_1 \tag{17a}$$

$$\begin{cases} E_{z2,n}(\rho,\phi,z)=\bar{A}_n\Omega_2 K_n(|k_2|\rho)\bar{F}_n \\ H_{z2,n}(\rho,\phi,z)=j\bar{A}_n\Omega_3 K_n(|k_2|\rho)\bar{F}_n \end{cases}, \quad \rho\geq\rho_1 \tag{17b}$$

and for $n=0$

$$\begin{cases} \psi_{z1,0}(\rho,\phi,z)=\bar{A}_0 J_0(k_1\rho)\bar{F}_0 \\ \psi_{z2,0}(\rho,\phi,z)=\bar{A}_0\Omega_2 K_0(|k_2|\rho)\bar{F}_0 \end{cases} \tag{18}$$

where

$$\psi_z=\begin{cases} E_z, & \text{if } \Delta(\bar{\beta})=B_1=\epsilon_{r1}\eta_1-\epsilon_{r2}\eta_2=0, \text{ TM modes} \\ H_z, & \text{if } \Delta(\bar{\beta})=A_2=\mu_{r1}\eta_1-\mu_{r2}\eta_2=0, \text{ TE modes} \end{cases}$$

In (17) and (18) for $n=0,\pm1,\pm2,\cdots$

$$\bar{A}_n=-j2k_0a_n/\left[\pi x^2J_n^2(x)\Delta'(\bar{\beta}_n)\right]$$

$$\bar{F}_n=\exp\left[jn(\phi-\phi_0)=jk_0\bar{\beta}_n z\right]$$

$$\Delta'(\bar{\beta}_n)=\frac{d}{d\bar{\beta}}\Delta(\bar{\beta})\bigg|_{\bar{\beta}=\bar{\beta}_n}$$

$$\eta_1=J_n'(x)/xJ_n(x)$$

$$\eta_2=H_n'^{(1)}(w)/WH_n^{(1)}(W)$$

$$\Omega_1=B_1/A_1,\ \Omega_2=J_n(x)/K_n(|w|) \text{ and } \Omega_3=\Omega_1\Omega_2$$

$$A_1=B_2=n\bar{\beta}(1/x^2-1/w^2). \tag{19}$$

For TE modes, $\bar{A}_0$ is given by $\bar{A}_0=2k_0b_0/[\pi x^2J_0^2(x)\Delta'(\bar{\beta}_0)]$. Since $\bar{\beta}_n\geqslant\bar{\beta}_r$ for guided modes, k_2 in (17) and (18) has been replaced by jk_2.

At a given frequency, only a finite number of modes are excited. These are the modes whose cutoff frequencies are lower than the operating frequency. The dominant HE_{11} mode is usually the first mode to be excited, because it has a zero cutoff frequency. Further, as long as the normalized frequency, defined as $V=k_0\rho_1(\epsilon_{r1}-\epsilon_{r2})^{1/2}$, is less than 2.405, the HE_{11} mode is the only surface-wave mode present except for an axially oriented on-axis dipole which excites the circularly symmetric modes only. For $V>2.405$, the HE_{21}, TM_{01}, and TE_{01} modes also begin to be excited. The number of excitable modes is determined by the cutoff conditions and the operating frequency. A detailed analysis of the cutoff conditions for a dielectric rod is given by Marcuse [12].

The total power carried by a guided mode is the sum of the powers in the positive and the negative z directions. It should be noted that the two powers are not, in general, equal.

$$P_s=|P_s(\bar{\beta}_n)|+|P_s(-\bar{\beta}_n)| \tag{20a}$$

where

$$P_s(\bar{\beta}_n)=\frac{1}{2(\mu_0\epsilon_0)^{1/2}}\int\int \mathrm{Re}\left[\vec{E}(\rho,\phi,z)\times\vec{H}^*(\rho,\phi,z)\right]\cdot\hat{z}\,dS. \tag{20b}$$

The integration is performed over the entire $z=0$ plane. Substituting (17) and (18) in (20), the total surface-wave power is obtained as

$$P_s=P_0(P_1-P_2)\cdot\begin{cases} (|a_n^z|^2+|a_n^\rho|^2+|a_n^\phi|^2), & n\geqslant1, \text{ hybrid modes} \\ (|a_0^z|^2+|a_0^\rho|^2), & n=0, \text{ TM modes} \\ (|b_0^\phi|^2), & n=0, \text{ TE modes} \end{cases} \tag{21}$$

where again the detailed expressions for P_0, P_1, and P_2 [11] are not given for the sake of brevity. It is, however, mentioned here that P_1 and P_2 are different for the three cases of hybrid, TM, and TE modes with $a_0^\phi=0$ for TM modes, and $b_0^z=b_0^\rho=0$ for TE modes.

For the special case of an on-axis dipole ($\rho_0=0$), it can be verified that all terms in the field and power expressions corresponding to $|n|>1$ are zero. Hence, in the radiation fields, radiated power and radiation pattern expressions, only terms corresponding to $n=0$ with J_z and $|n|=1$ with J_ρ and J_ϕ are present in the infinite series (for radiation pattern $m=0,1$ too). Moreover, an on-axis dipole does not excite hybrid modes with azimuthal number greater than 1. It should be noted that at $\rho_0=0$, $a_1^z=a_0^\rho=a_0^\phi=b_0^\phi=0$. Hence, the axial component J_z gives rise to the circularly symmetric TM modes, while the transverse components J_ρ and J_ϕ produce the hybrid dipolar modes ($|n|=1$). In other words, an on-axis and axially oriented dipole excites TM_{0m} modes only. Further, the radiation pattern of this dipole does not vary with ϕ ($n=m=0$) and is symmetric about $\theta=\pi/2$ plane. On the other hand, an on-axis transverse dipole excites HE_{1m} and EH_{1m} modes only and the corresponding radiation pattern is symmetric about $\theta=\pi/2$ with a period of π in ϕ.

IV. Dipole in the Cladding Region

When the dipole is in the cladding region, $\rho_0>\rho_1$, the fields and the power expressions may be deduced from the existing equations by making appropriate changes. Since these expressions are quite messy, no attempt is made here to present them in details although details are available [11]. The principal terms in the analysis a_{n1}, b_{n1}, a_{n2}, b_{n2}, Δ_0, a_n, and b_n have to be adjusted. The expressions for S_n, R_n, S_n', and R_n' can be obtained from those in (10), where Y_n should be replaced by $H_n^{(1)}$, ϵ_{r1} by ϵ_{r2}, k_1 by k_2, v_1 by $v_2=k_2\rho_0$,and T_0 by $T_0/j=k_2(\mu_0)^{1/2}/4$. All other variables such as $A_1,A_2,B_1,B_2,\eta_1,\eta_2,\Delta(\bar{\beta})$, etc., are the same as before. The radiation fields, radiated power, and radiation pattern may be obtained from (14), (15a), and (15b), respectively, provided that a_{n2} is substituted by $a_{n2}+R_n'$ and b_{n2} by $b_{n2}+S_n'$ in them. The results for this case may be simplified, in a manner similar to the case $\rho_0<\rho_1$, by decomposing $a_{n2}+R_n'$ and $b_{n2}+S_n'$ into three parts involving J_z, J_ρ, and J_ϕ. The derivation of the simplified results is quite straightforward.

The surface-wave fields are obtained from (17) and (18), and the total surface wave power from (21) provided that the changed expressions $\bar{A}_n$, $\bar{A}_0$, and P_0 for $\rho_0>\rho_1$ are used in them.

V. Scattering Due to a Localized Inhomogeneity

There has been considerable interest in reducing the attenuation caused by absorption and scattering losses in a cladded fiber. Here, we shall study scattering losses due to the presence of minute inhomogeneities or metallic impurities in the glass. When light is guided inside a fiber, these scattering centers cause losses by radiation and mode conversion.

We shall now apply the analyses developed in the previous sections to the scattering problem. It is assumed that the scatterer is small compared with the incident wavelength and the size of the fiber, conditions that are usually met in practice [13]. In what follows, scattering due to an inhomogeneity of volume Δv and permittivity difference $\Delta\epsilon = \epsilon_0 \Delta\epsilon_r$ is studied. The inhomogeneity is assumed to be located at ρ_0 and ϕ_0 in the $z=0$ plane. Since the inhomogeneity is a small perturbation in the permittivity of the dielectric material and occupies a small volume Δv, the fields of the incident mode are only slightly perturbed. Thus, the Maxwell's equation in Δv can be written as

$$\nabla x\vec{H} = -jk_0\epsilon_{ri}\vec{E} + \vec{J}, \qquad i=1 \text{ or } 2 \tag{22a}$$

where

$$\vec{J} = -jk_0\Delta\epsilon_r\vec{E} \simeq -jk_0\Delta\epsilon_r\Delta v\delta(\vec{\rho}-\vec{\rho}_0)\vec{E}^i. \tag{22b}$$

E^i is the incident electric field with components $E^i_\rho = q_\rho(\rho)\cos n\phi$, $E^i_\phi = q_\phi(\rho)\sin n\phi$ and $E^i_z = q_z(\rho)\cos n\phi$, and $\Delta\epsilon_r = \epsilon_s - \epsilon_{ri}$ where $\epsilon_{ri} = \epsilon_{r1}$ if the inhomogeneity is in the core and $\epsilon_{ri} = \epsilon_{r2}$ if it is in the cladding. $q(\rho)$ is a function of ρ only. The normalized radiated power can be expressed as $\bar{P}_r = P_r/(\Delta\epsilon_r\Delta\bar{v})^2 P_i$, where P_i is the incident modal power given by (20b) in which $\vec{E}$ and $\vec{H}$ are substituted by those of the incident mode, $\Delta\bar{v} = \Delta v/\rho_1^3$ is the normalized volume of the inhomogeneity and P_r is obtained from (16). Similarly, the normalized surface-wave power scattered into a particular mode is given by $\bar{P}_s = P_s/(\Delta\epsilon_r\Delta\bar{v})^2 P_i$, where P_s is obtained from (21). Although the analyses developed in this paper are sufficiently general to enable us to study radiation and mode conversion from any arbitrary incident mode into any scattered mode, we shall, for the simplicity of presentation and illustration, only concentrate on the case of the fiber operating in the dominant HE_{11} mode and power scattered into several lower order modes.

The variation of the normalized radiated power with frequency for several values of ρ_0/ρ_1 is shown in Fig. 4. The fiber has relative permittivities $\epsilon_{r1} = 2.341$ and $\epsilon_{r2} = 2.250$ and permeabilities all equal to unity. The incident mode is taken to be HE_{11} and the angular position of the inhomogeneity zero. The behavior of the radiated power is largely determined by the variation in the incident field strength. Thus as frequency increases the power for $\rho_0/\rho_1 < 1$ increases, whereas for $\rho_0/\rho_1 > 1$ it decreases after reaching a maximum. This is due to the fact that as the frequency increases, the incident surface-wave fields and hence power become more and more confined to the core, but decay exponentially in the outer cladding region.

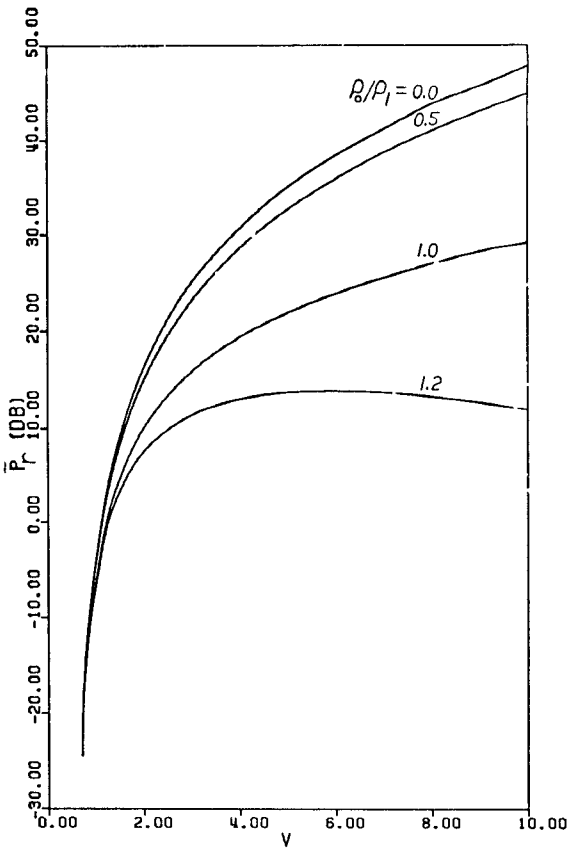

Fig. 4. Normalized radiated power $\bar{P}_r$ versus normalized frequency V.

Next, we examine the radiation patterns at $V=2.0$. As mentioned earlier, when all three components of the current density are present, there is no symmetry in the pattern, thus θ and ϕ should be varied in full ranges of 0° to 180° and 0° to 360°, respectively. However, if $J_z = 0$ or $J_\rho = J_\phi = 0$, it can be verified that the radiation patterns become symmetric about $\theta = 90°$. A large variety of patterns may be produced for various values of ρ_0 and ϕ_0. Here, we confine ourselves to an example in which all components of the current are present. Let us choose $\phi_0 = 30°$ and $\rho_0/\rho_1 = 0.5$ and let $\bar{P}(\phi,\theta)$ denote the radiation pattern normalized to unity. Figs. 5(a), (b), (c), and (d) illustrate the patterns in $\phi = 0°$, 90°, 180°, and 270° planes, respectively, while Fig. 5(e) shows the pattern in $\theta = 90°$ plane with ϕ varying from 0° to 360°. Excellent symmetry is observed about $\theta = 90°$ in all patterns in $\phi =$ const. planes. This is explained by the fact that the axial component of the induced current is much smaller than the transverse ones ($J_z/J_\rho = 0.06$ and $J_z/J_\phi = 0.11$). On the other hand, since J_z has a nonzero value, there is a slight but still visible asymmetry in these patterns. All patterns have nulls at $\theta = 0°$ and $\theta = 180°$ and a number of peaks. $\bar{P}(\phi, 90°)$, as expected, shows no symmetry at all.

Figs. 6 and 7 show the variation of the normalized scattered power for several lower order modes versus

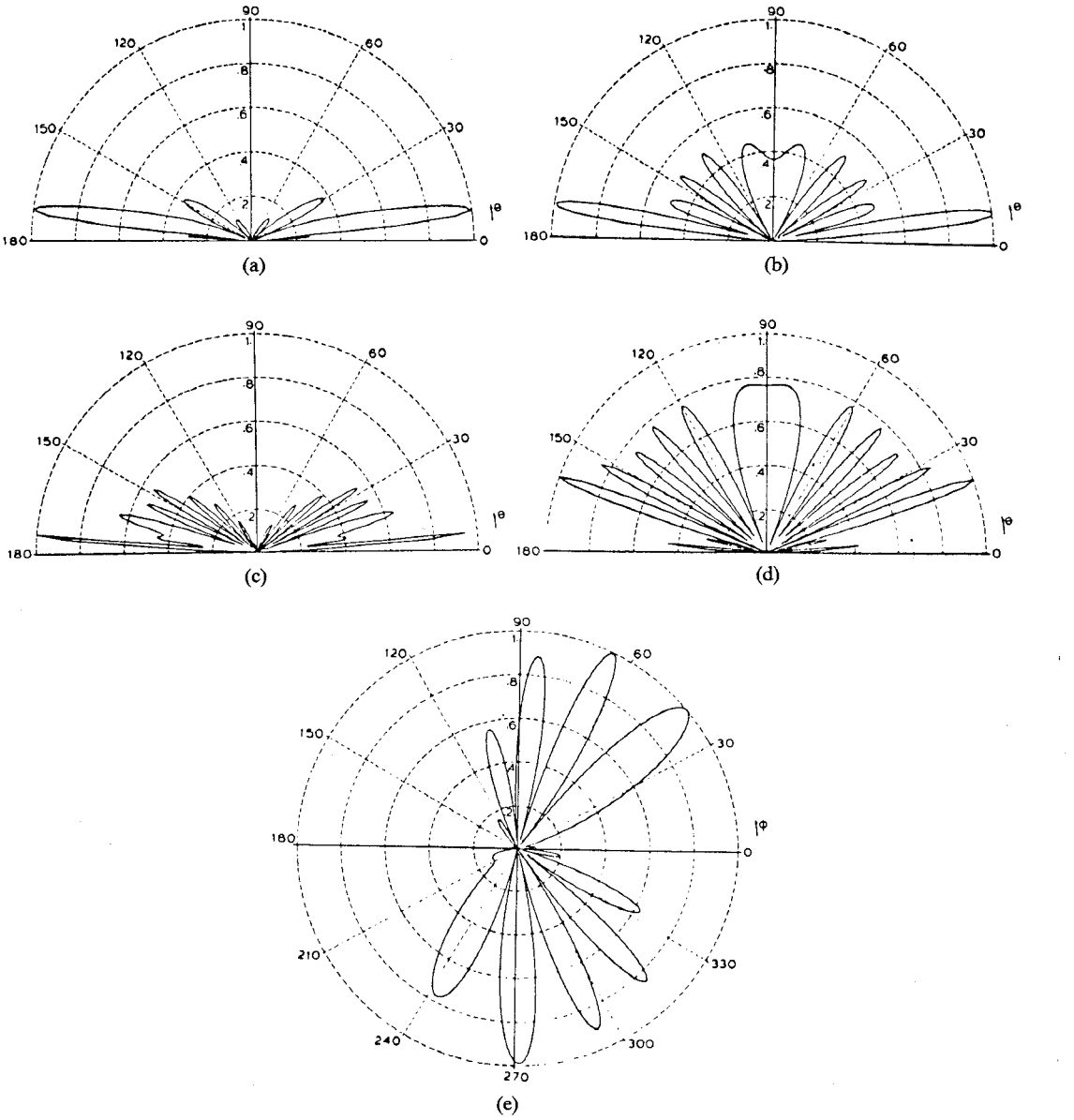

Fig. 5. Radiation patterns $\bar{P}(\phi,\theta)$ at $V=2.0$, $\rho_0/\rho_1=0.5$ and $\phi_0=30°$. (a) $\bar{P}(0°,\theta)$, (b) $\bar{P}(90°,\theta)$, (c) $\bar{P}(180°,\theta)$, (d) $\bar{P}(270°,\theta)$, (e) $\bar{P}(\phi,90°)$.

frequency. Fig. 6(a) illustrates the variation of power for the scattered HE_{11} mode. Again, for $\rho_0/\rho<1$, the power increases with frequency, whereas for $\rho_0/\rho_1>1$, it decreases rapidly after reaching a maximum. This can be explained by the same reason advanced for the radiated power. Variations of power for the scattered HE_{12} and EH_{11} modes are shown in Figs. 6(b), (c) and for the TM_{01}, HE_{21} and HE_{31} modes in Figs. 7(a), (b), (c), respectively. Their general behavior is similar to the HE_{11} mode. However, for $\rho_0/\rho_1=0.5$, the HE_{12} mode exhibits a peculiar behavior. After an initial increase, its power drops to -30.1 dB at $V=7$, and then rises to -0.38 dB at $V=10$. This drop in power is caused by the fact that the field strength of this mode for certain values of ρ_0, ϕ_0, and V becomes very small. This effect is much more pronounced in Fig. 8 which shows variations of surface-wave powers with ρ_0/ρ_1 at $V=5$. It can be seen in Figs. 6, 7, and 8 that at $\rho_0/\rho_1=0$ the HE_{11} and HE_{12} modes are excited much more strongly than the EH_{11} mode, and the HE_{21}, HE_{31}, and TM_{01} modes whose azimuthal numbers differ from one are not excited at all. The curves for the HE_{21} and TM_{01} modes completely overlap due to their degeneracy.

It should be emphasized that not only does the scattered power depend on ρ_0, but also on ϕ_0. For fibers with $\epsilon_{r1}\simeq\epsilon_{r2}$, the axial component of the incident electric field is much smaller than the transverse ones which are in turn nearly equal; i.e., $q_z(\rho)\ll q_\rho(\rho)\simeq q_\phi(\rho)$. Hence, the power scattered into hybrid modes and the radiated power vary slightly with ϕ_0. The power of TM modes depend on E_z^i and E_ρ^i only, hence for angular positions other than zero degree, the power of the TM_{01} mode is lower than that of the HE_{21} mode and for the special case of $\phi_0=90°$ it ceases to be excited, while the TE_{01} mode is excited maximally.

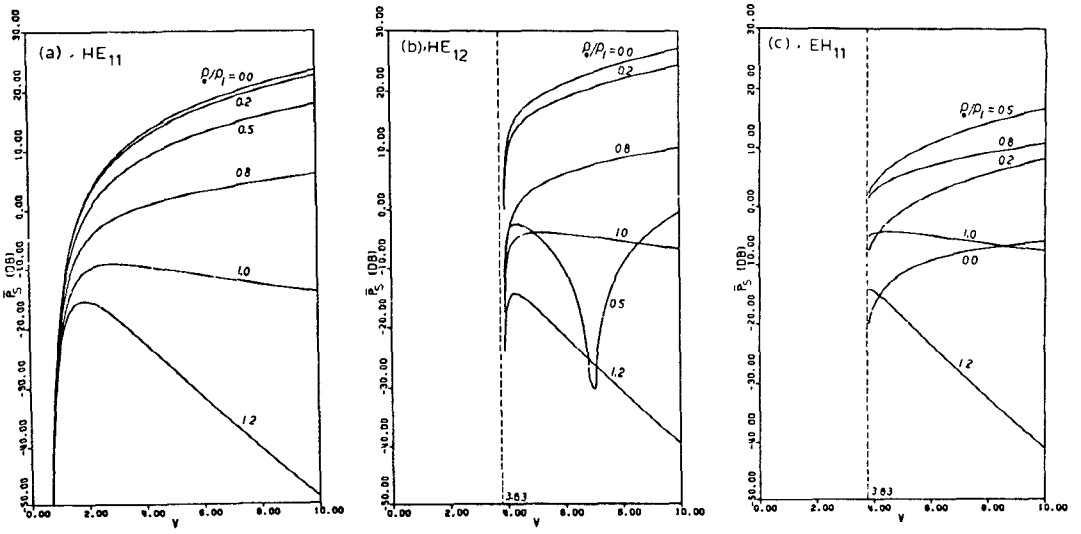

Fig. 6. Normalized scattered surface-wave modal power $\bar{P}_s$ versus normalized frequency V. (a) HE_{11}, (b) HE_{12}, (c) EH_{11}.

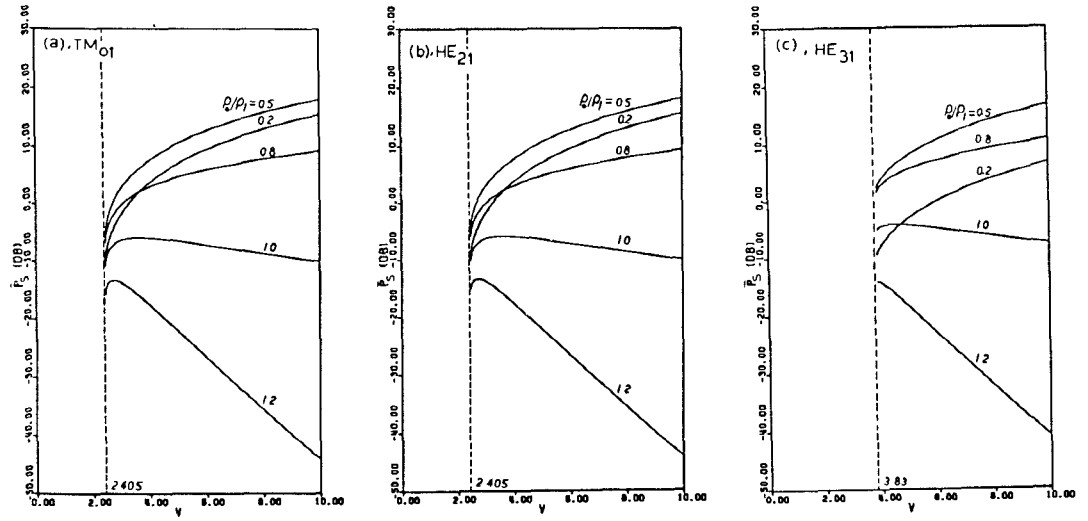

Fig. 7. Normalized scattered surface-wave modal power $\bar{P}_s$ versus normalized frequency V. (a) TM_{01}, (b) HE_{21}, (c) HE_{31}.

Comparisons were also made with the numerical results for the total radiated power calculated from the expression based on the infinite medium approximation given by $P=(\pi/3)(\mu_0/\epsilon_1)^{1/2}\cdot(\Delta v|\vec{J}|/\lambda)^2$; λ being the wavelength. Computations were carried out for the cases $\rho_0/\rho_1=0.0$, 0.5, 1.0, and 1.2 while V is varied from 0.7 to 10. In all cases, the results of the present exact analysis are very close to those of the infinite medium approximation. This clearly establishes the accuracy of the infinite medium approximation when the dielectric difference between the core and the infinite cladding is small. However, when the dielectric difference is not small, the infinite medium approximation is no longer valid. Further, the exact analysis yields radiation patterns which are markedly different from the doughnut shape patterns predicted in the infinite medium approximation. The results for the guided wave power are identical to those obtained using the Lorentz reciprocity theorem, hence comparisons of the computed guided modal powers are unnecessary.

VI. Conclusions

A rigorous Green's function formulation for the problem of an arbitrarily oriented and off-axis point electric dipole in a two-layer cylindrical dielectric waveguide has been carried out, and permits the corresponding field solutions for both the radiation and guided modes to be obtained. The practical significance of these solutions is demonstrated through the immediate application of these solutions to the problem of radiation and mode conversion due to an arbitrarily located and off-axis inhomogeneity in a step-index optical fiber waveguide. So far as the total radiated power is concerned, the results in the infinite-medium approximation are sufficiently good, provided that the dielectric difference between the core and the cladding is sufficiently small. Nevertheless, the Green's function formulation of the present paper leads to exact results, against which the accuracy of the infinite-medium approximation can be checked in cases where the

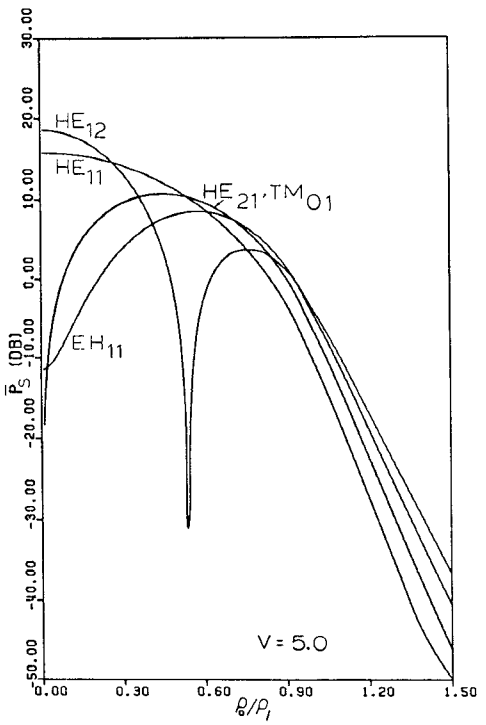

Fig. 8. Normalized scattered surface-wave modal power versus ρ_0/ρ_1 for the HE_{11}, HE_{12}, EH_{11}, HE_{21}, and TM_{01} modes at $V=5$.

dielectric difference is not necessarily small. The results for the guided modal power are identical to those obtained using the Lorentz reciprocity theorem. However, the spatial distribution of scattered light intensity, or radiation pattern, calculated here differs markedly from that obtained in the infinite-medium approximation, which does not predict multiple peaks. These radiation patterns provide the possibility of being checked experimentally.

The method of analysis is generally applicable to multilayer cylindrical dielectric structures. We have already extended the analysis to such three-layer structures as the cladded fiber, the dielectric tube and the W-type fiber. The results will be represented later. It also goes without saying that the present analysis can be applied to similar structures used in millimeter wave communications.

References

[1] L. B. Felsen and N. Marcuvitz, *Radiation and Scattering of Waves*. Englewood Cliffs, NJ,: Prentice Hall, 1973.

[2] J. A. Kong, *Theory of Electromagnetic Waves*. New York: Wiley, 1975.

[3] J. W. Duncan, "The efficiency of excitation of a surface wave on a dielectric cylinder," *IRE Trans. Microwave Theory Tech.*, vol. MTT-7, pp. 257–268, Apr. 1959.

[4] J. Brown and H. S. Stachera, "The launching of an axial cylindrical surface wave," *Proc. Inst. Elec. Eng.*, vol. 109c, pp. 18–25, Mar. 1962.

[5] G. L. Yip, "Launching efficiency of the HE_{11} surface wave mode on a dielectric rod," *IEEE Trans. Microwave Theory Tech.*, vol. MTT-18, pp. 1033–1041, Dec. 1970.

[6] G. Goubau, "On the excitation of surface waves," *Proc. IRE*, vol. 40, pp. 865–868, July 1952.

[7] R. E. Collin, *Field Theory of Guided Waves*. New York: McGraw-Hill, 1960, ch. 11, p. 483.

[8] P. J. B. Clarricoats and K. B. Chan, "Propagation behaviour of cylindrical dielectric-rod waveguides," *Proc. Inst. Elec. Eng.*, vol. 120, no. 11, pp. 1371–1378, 1973.

[9] A. W. Snyder, "Excitation and scattering of modes on a dielectric or optical fiber," *IEEE Trans. Microwave Theory Tech.*, vol. MTT-17, pp. 1138–1144, Dec. 1969.

[10] G. N. Watson, *A Treatise on the Theory of Bessel Functions*, Cambridge, England: Cambridge Univ. Press, 1966, p. 361.

[11] A. Safaai-Jazi, "A study of mode classification and scattering from an off-axis inhomogeneity in step-index optical fibers," Ph.D. dissertation, Dep. Elec. Eng., McGill Univ., Montreal, P.Q., Canada, May 1978, ch. 4.

[12] D. Marcuse, *Light Transmission Optics*. New York: Van Nostrand, 1972, ch. 8.

[13] F. P. Kapron, D. B. Keck, and R. D. Maurer, "Radiation losses in glass optical waveguides," *IEE Conf. Publ.* pp. 148–153, 1970.